Available online at www.sciencedirect.com
ScienceDirect
Chinese Journal of Aeronautics 23(2010) 327-333
Chinese Journal of Aeronautics
www.elsevier.com/locate/cja

Multi-frequency RCS Reduction Characteristics of Shape Stealth with MLFMA with Improved MMN

Liu Zhanhe[a], Huang Peilin[a,*], Gao Xu[b], Li Ying[a], Ji Jinzu[a]

[a]*School of Aeronautic Science and Engineering, Beijing University of Aeronautics and Astronautics, Beijing 100191, China*

[b]*The First Aircraft Institute, Aviation Industry Corporation of China, Xi'an 710089, China*

Received 15 June 2009; accepted 9 January 2010

Abstract

Three new control factors are presented for calculating the multipole mode number (MMN) efficiently and precisely. The effects of these control factors on the number of integral samples and the precision of multilevel fast multipole algorithm (MLFMA) are investigated. A new approach based on control factors which is proven to be able to improve the computational efficiency and reduce the needed memory significantly as well as ensuring the proper precision. For three aircraft models, the improved MLFMA is employed to analyze their multi-frequency scattering characteristics. It is found that aircraft shape can influence radar cross section (RCS) in different frequency zones. Both the multi-frequency RCS reduction characteristics of shape stealth aircraft and the conventional aircraft with stealth design taken into account are investigated, and the results show that shape stealth exhibits significant RCS reduction in the resonance and high-frequency zones, and with a weaker influence in the Rayleigh zone. Compared with radar absorbing material (RAM), shape stealth yields a wider multi-frequency RCS reduction. The above-mentioned results can be applied to stealth design for multiple frequencies or even for all frequencies.

Keywords: radar cross section; reduction; electromagnetic wave; scattering; aircraft

1. Introduction

Aircraft stealth technology can significantly reduce the enemy's detection probability and increase the concealment capacity[1]. Currently, stealth technology offers wide applications, and have become a vital tactical tool for designing new-generation aircraft[2]. For stealth aircraft, the radar cross section (RCS) calculation methods[3-4] must achieve high precision because of typically low RCS values. Multilevel fast multipole algorithm (MLFMA)[5-8] has found wide applications in RCS calculations owing to its excellent accuracy in solving integral equations without the introduction of boundary conditions[9].

To calculate the RCS for the whole aircraft, a new concept utilizing three control factors is presented, and the effects of these control factors on the number of integral samples and the precision of the MLFMA are investigated in detail. This new approach is used to increase the computing efficiency rapidly and save memory while ensuring the same precision. Numerical computations show that the improved measurement approach is accurate and effective.

With further developments in radar techniques, particularly in new radar systems, the detection range has been extended to low frequencies (e.g. the Rayleigh zone). Therefore, stealth design of aircraft, tanks and ships faces greater challenges. The electromagnetic waves scattering characteristics of aircraft have been discussed in some literatures based on flat plate models[10], but the whole-aircraft RCS characteristics and the reduction characteristics of multiple frequencies (or all frequencies) have not been addressed. In order to acquire information on multiple frequencies, an improved MLFMA is employed and the RCS reduction characteristics of shape stealth techniques are investigated based on three different aircraft models in the Rayleigh zone, resonance zone and high-frequency zone. Compared with radar absorbing materials (RAMs), the shape stealth technique reveals advantages. These three aircraft models are traditional Configuration 1, traditional Configuration 2 with stealth design taken into consideration, and shape stealth Configuration 3, which are described in Fig.1. To eliminate

*Corresponding author. Tel.: 86-13241815191.
E-mail address: peilin_h@buaa.edu.cn
Foundation item: National Basic Research Program of China (61320)

doi: 10.1016/S1000-9361(09)60223-5

the scale effect of aircraft, all configurations are set to the typical dimension of 1 m in length.

(a) Configuration 1

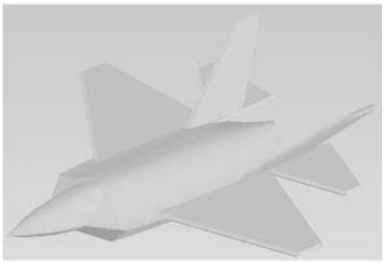

(b) Configuration 2

(c) Configuration 3

Fig.1 Different configurations of aircraft models.

2. Basic Theory of MLFMA

Combined field integral equation (CFIE)[9] is employed to accelerate the convergence and effectively solve the stability problems when it is in the inner resonance frequency. The problem of scattering from perfect conductive objects (such as aircraft and missiles) can be solved with CFIE, which can be transformed into a linear matrix vector equation by modeling the object surface with patches and expanding the current with roof-top basis functions[11]. The basic principle of fast multipole method (FMM) is that CFIE can be described as[7-8]

$$F_j = \sum_{n\in G_N}\sum_{i\in G_n} Z_{ji}a_i + \frac{ik}{4\pi}\int \mathrm{d}^2(\hat{\boldsymbol{k}}\boldsymbol{V}_m(\hat{\boldsymbol{k}}))\cdot \sum_{n\in G_F}\alpha_{mn}(\hat{\boldsymbol{r}}_{mn}\cdot\hat{\boldsymbol{k}})\sum_{i\in G_n}\boldsymbol{W}_n^*(\hat{\boldsymbol{k}})a_i \qquad j\in G_m \tag{1}$$

where α_{mn} is the translation operator, Z_{ji} the matrix element produced by the jth and ith variables, a_i the current factor, G_N the near groups, G_F the far groups, G_n the nth group, G_m the mth group, $\hat{\boldsymbol{r}}_{mn}$ the unit vector between mth and nth groups, $\hat{\boldsymbol{k}}$ the unit wave vector, k the wave number, and $\boldsymbol{V}_m(\hat{\boldsymbol{k}})$ and $\boldsymbol{W}_n^*(\hat{\boldsymbol{k}})$ are the receiving pattern and the radiation pattern respectively.

Then the computation process of matrix vector products is divided into two parts: the near interaction between nearby sources and the far interaction between well-separated ones.

In Eq.(1), the near interaction is calculated with the method of moment (MOM)[12], and the far interaction is divided with MLFMA into three phases: aggregation (or upward) phase, translation phase and disaggregation (or downward) phase.

In the aggregation phase, the outgoing pattern is computed at the finest level by calculating the radiation patterns of corresponding sources, while a coarser level calculation of the outgoing pattern is obtained through interpolation and shift from its child level. The incoming pattern of both top and lower levels is obtained through anterpolation[13-14].

3. Novel Control Factors of Multipole Mode Number (MMN)

3.1. Proposition of control factors

The MMN L, which is the number of multipole expansions needed to represent the spectral content of the radiation pattern, influences the interpolation precision and the integral sampling[14]. With traditional MLFMA, L is doubled and the number of integral samples expressed as $K = 2L^2$ is increased by a factor of four from the finer level to the coarser level. L is represented by the experimental formula as[15]

$$L = kD + \ln(kD + \pi) \tag{2}$$

where D is the length of the cube (which enclose the related patches) diagonal line. Eq.(2) is applied to every level to reduce the memory[15].

In this article, to improve precision, the refined formula[16] is introduced at every level and expressed as

$$L_l = kD_l + 1.8(d_0)^{2/3}(kD_l)^{1/3} \tag{3}$$

where the value of d_0 depends on the desired accuracy and worst of which is $D_l = 1.732a_l$, and a_l is the side length of the cube of level l.

It is shown that, for a given cube at level l, a reasonable L_l can be calculated and used to terminate the infinite item in MLFMA. As a result, the number of integral samples for each level, described as $K_l = 2L_l^2$, will be obtained and the related memory will be adjusted.

Eq.(3) can be transformed to

$$L_l = L_1 + L_2 \tag{4}$$

where $L_1 = kD_l$ and $L_2 = 1.8(d_0)^{2/3}(kD_l)^{1/3}$. For a given incident wavelength λ, $L_1 \propto O(D_l)$ and $L_2 \propto O(d_0^{2/3})$,

$D_l^{1/3}$) respectively.

To calculate MMN effectively, three control factors α, β and γ are introduced. The three parts within L_1 and L_2 can be controlled freely through adjusting these control factors. A modified formula of Eq.(3) can be described as

$$L_l = \alpha kD_l + 1.8(\beta d_0)^{2/3}(\gamma kD_l)^{1/3} \tag{5}$$

To investigate the effects of the MMN and the cube size on the computational precision of each level, d_0 is described as

$$d_0 = \left[\frac{L_l - \alpha kD_l}{1.8(\gamma kD_l)^{1/3}}\right]^{3/2} \frac{1}{\beta} \tag{6}$$

Precision of MLFMA is related to the MMN and the cube size of corresponding level. By increasing the value of L_l, the precision can be enhanced, but the memory will be increased rapidly owing to the increase of integral sampling number. Therefore, the MMN should be decreased when the appropriate precision is achieved.

Generally, d_0 is a natural number and $d_0 = 1$ gives the accuracy of 0.1. L_l is a series of discrete numbers correspondingly calculated with Eq.(3), and the control factors can make it continuous. During the aggregation and disaggregation phases, the magnitude of errors will be growing when interpolating from the finer level to the coarser level, so the error at the finest level is most important to MLFMA precision. Thus, high precision at the finest level must be achieved while precision at other levels can be relaxed to improve the efficiency, reduce the number of integral samples, and save the additional memory.

Based on these control factors, a new approach is proposed to ensure the precision and improve the efficiency. To ensure precision at the finest level, the numbers of interpolating nodes and integral samples are fixed or decreased slightly with higher values of α, β and γ; at other levels, the control factors α, β and γ are used to decrease the MMN. That is, the control factors can be changed according to different levels and should be increased only when achieving very high precision is needed.

3.2. Effects of control factors on number of integral samples

The novel approach proposed above is employed to analyze the characteristics of the three control factors. At level l, the ranges of α, β and γ are defined within 0.6-1.0 to reduce their influences on computing precision.

The aircraft model of Configuration 3 (shown in Fig.1(c)) is selected to investigate the effects of α, β and γ on K_l. Fig.2 shows the curve of K_l changing with α, β and γ when the aircraft is illuminated by a uniform plane wave of 14 GHz, where the electrical size is 47λ and the number of total levels is 7.

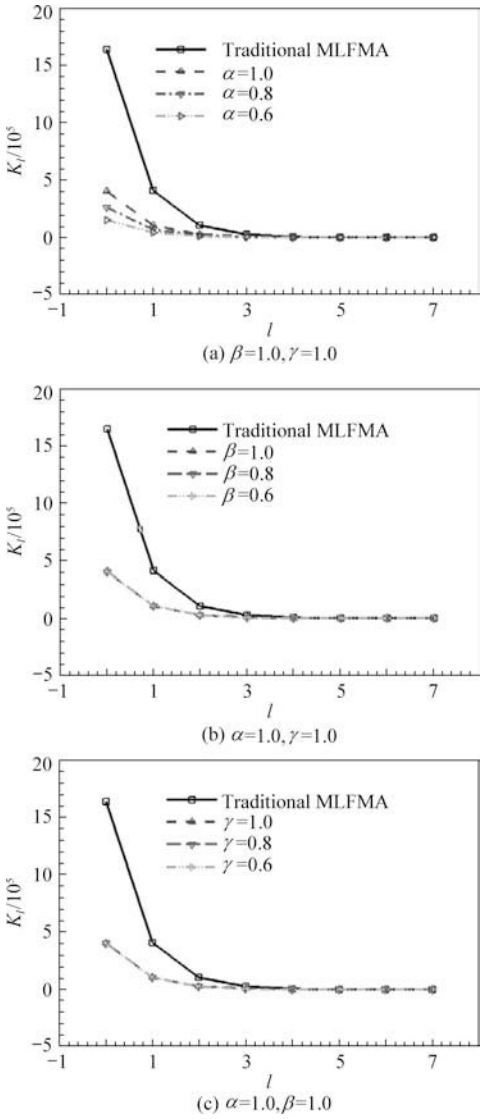

(a) β=1.0, γ=1.0

(b) α=1.0, γ=1.0

(c) α=1.0, β=1.0

Fig.2 Effects of α, β and γ on number of integral samples.

Fig.2(a) shows that α has significant influence on K_l at different levels when β = 1.0 and γ = 1.0. At the finest level (l=7), the same number of integral samples is used. At other levels, K_l decreased at each level because of the decline of control factor α. For the improved approach, K_l is smaller than that for the conventional MLFMA, and 556 MB of memory is saved when α = 0.6.

Fig.2(b) shows the curves of K_l changing with different β when α = 1.0 and γ = 1.0, from which it can be seen that β has an imperceptible influence on K_l for different levels. Furthermore, at several coarser levels, Eq.(5) shows that the number of integral samples is decreased with the reduction of β.

Fig.2(c) shows the curves of K_l changing with different γ when α = 1.0 and β = 1.0, where the trend of curves is similar to that in Fig.2(b). It is seen that γ has an imperceptible influence on K_l. However, Eq.(5)

shows that the number of integral samples is decreased at coarser levels.

Fig.2 indicates that the control factor α affects K_l significantly while the effects of the other two factors are insignificant. It is also shown that the value of K_l obtained with the improved approach is less than that required by the traditional MLFMA. Therefore, for calculating aircraft RCS, α should be decreased greatly to reduce the number of integral samples and to save the memory while the appropriate precision is ensured and all the control factors are adjusted to obtain higher precision.

3.3. *Effect of control factors on precision and efficiency of MLFMA*

(1) RCS arithmetic mean errors (AME) and geometric mean errors (GME)

To investigate the precision of improved MLFMA, the RCS AME and GME are employed. It is presumed that *a* and *b* are azimuths, and *N* is the RCS calculation sampling number of angle zone (*a*, *b*). Then the RCS arithmetic mean (AM) of angle zone (*a*, *b*) can be expressed as

$$\mathrm{AM}_{(a,b)} = 10\lg\left(\frac{1}{N}\sum_{i=1}^{N}\sigma_{i,\mathrm{m}^2}\right) \tag{7}$$

where σ_{i,m^2} is the RCS of *i*th azimuth, m^2. Meanwhile, the RCS geometric mean (GM) can be expressed as

$$\mathrm{GM}_{(a,b)} = 10\lg\sqrt[N]{\prod_{i=1}^{N}\sigma_{i,\mathrm{m}^2}} \tag{8}$$

Thus, the AME and GME between computational and experimental results are

$$\mathrm{AME}_{(a,b)} = \left|\mathrm{AM}_{(a,b),\mathrm{MLFMA}} - \mathrm{AM}_{(a,b),\mathrm{experiment}}\right| \tag{9}$$

$$\mathrm{GME}_{(a,b)} = \left|\mathrm{GM}_{(a,b),\mathrm{MLFMA}} - \mathrm{GM}_{(a,b),\mathrm{experiment}}\right| \tag{10}$$

where the subscripts (MLFMA and experiment) indicate the corresponding methods for determining the AM or GM.

(2) Analysis on the precision and efficiency of improved MLFMA

To validate the higher efficiency and accuracy of the improved MLFMA, both traditional MLFMA and the improved MLFMA with different control factors are employed to calculate the RCS of Configuration 3. All the numerical results are compared with experimental values when the frequency of the uniform plane wave is 10 GHz and the electrical size is 33λ. To analyze the stealth performance of aircraft, the RCS of *i*th azimuth (dBsm) can be described as

$$\sigma_{i,\mathrm{dBsm}} = 10\lg\sigma_{i,\mathrm{m}^2} \tag{11}$$

Table 1 shows parameters (such as memory and time) involved in the traditional MLFMA and the improved MLFMA. Fig.3 shows the comparison curves of RCS for computational and experimental results. Table 2 shows the RCS AME and GME corresponding to experimental results. In Fig.3 and Tables 1-2, (α, β, γ) denotes the corresponding amplitude of α, β and γ.

Table 1 Parameters of traditional and improved MLFMA for Configuration 3

Method	(α, β, γ)	Memory/MB	Time/s
Traditional MLFMA		974	402 536
Improved MLFMA	(1.0, 1.0, 1.0)	692	313 693
	(0.9, 0.9, 0.9)	563	263 728
	(0.8, 0.8, 0.8)	543	258 851
	(0.7, 0.7, 0.7)	432	228 690
	(0.6, 0.6, 0.6)	363	97 217

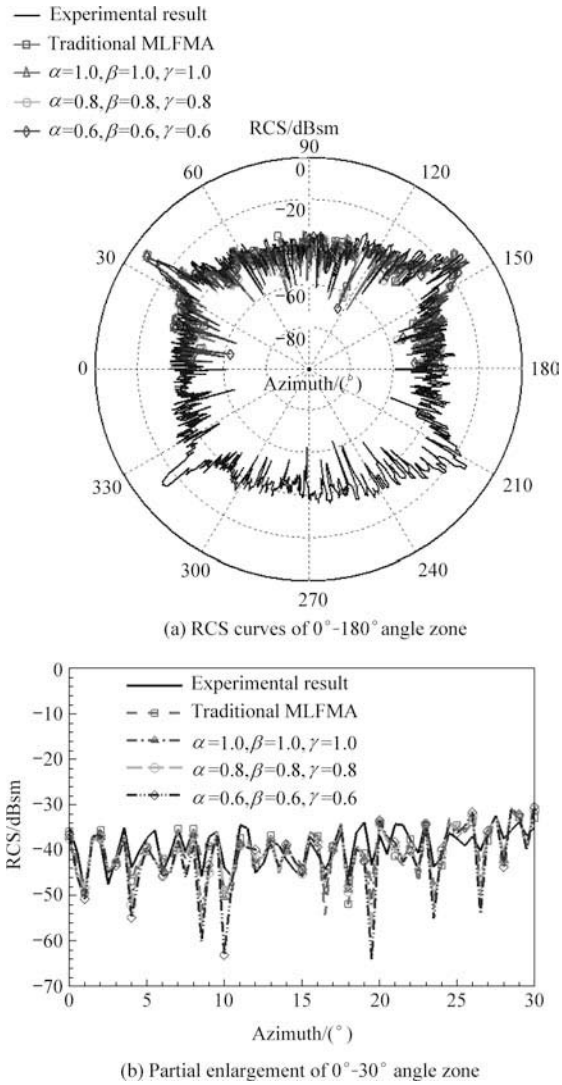

(a) RCS curves of 0°-180° angle zone

(b) Partial enlargement of 0°-30° angle zone

Fig.3 RCS curves of computational and experimental results.

Table 2 RCS AME and GME of traditional and improved MLFMAs for Configuration 3

Method	(α,β,γ)	0°-30°		0°-180°	
		AME/dB	GME/dB	AME/dB	GME/dB
Traditional MLFMA		1.545 9	0.821 0	0.973 0	1.208 7
Improved MLFMA	(1.0,1.0,1.0)	1.282 7	1.000 4	0.832 5	1.323 8
	(0.9,0.9,0.9)	1.440 0	1.444 1	0.948 0	1.341 8
	(0.8,0.8,0.8)	1.481 8	1.737 8	0.971 2	1.326 8
	(0.7,0.7,0.7)	1.554 6	1.870 5	0.961 9	1.372 7
	(0.6,0.6,0.6)	1.343 2	2.119 2	0.997 0	1.394 5

Table 1 shows that the memory requirements of the improved MLFMA are decreased significantly following the adjustment of control factors. The memory usage of traditional MLFMA is 974 MB while that of the improved MLFMA is reduced to 692, 563, 543, 432, 363 MB separately, and resulting in a savings of 282, 411, 431, 542, 611 MB respectively. Computational time is decreased greatly owing to memory reduction. For instance, the time for (0.6, 0.6, 0.6) is reduced to be less than 25% of the time used by the traditional MLFMA, and the corresponding efficiency is increased by three times.

For the precision analysis, the computational curves are remarkably consistent with the experimental results as shown in Fig.3(a). When (α, β, γ) is chosen from the range of (0.6, 0.6, 0.6) to (1.0, 1.0, 1.0), Table 2 indicates that the errors of the improved MLFMA are close to those of the traditional MLFMA for two angle zones of 0°-30° and 0°-180°. All the RCS AME values related to the experimental results are suitable enough for analyzing the stealth performance of an aircraft.

On the other hand, the RCS GME increases with the decrease of control factor values, which implies that MLFMA precision will become slightly worse, as indicated in Table 2. To prove this, the partial enlargement of 0^o-30^o angle zone is shown in Fig.3(b). It can be seen that the trends of all curves are fairly consistent and the control factors have imperceptible effect on precision. At some wave hollows (such as around 10° or 19.5°), the precision becomes worse while the control factors vary from (1.0, 1.0, 1.0) to (0.6, 0.6, 0.6). As a result, the changes of precision due to the decline of control factors are acceptable for whole-aircraft RCS computations.

Therefore, the control factors are chosen within the range between (0.6, 0.6, 0.6) and (1.0, 1.0, 1.0) for whole-aircraft RCS computations in order to ensure appropriate precision, improve efficiency, and save memory. Fig.3(a) and Tables 1-2 show that the improved MLMFA can enhance efficiency rapidly, save considerable memory, and extend the range of computational frequencies. In addition, different control factors can be selected at different levels to adjust the precision.

4. Multi-frequency RCS Reduction Characteristics of Shape Stealth

In this article, improved MLFMA is applied to investigate the multi-frequency RCS reduction characteristics of shape stealth in Rayleigh, resonance, and high frequency zones.

4.1. Shape effects of aircraft on multi-frequency RCS

To analyze the RCS reduction characteristics of whole-aircraft, the shape effects on multi-frequency RCS values should be investigated first. Fig.4 shows the curves of Configuration 3 in three frequency zones: the Rayleigh zone (f = 0.28 GHz), the resonance zone (f = 0.70 GHz), and the high-frequency zone (f = 7.00 GHz).

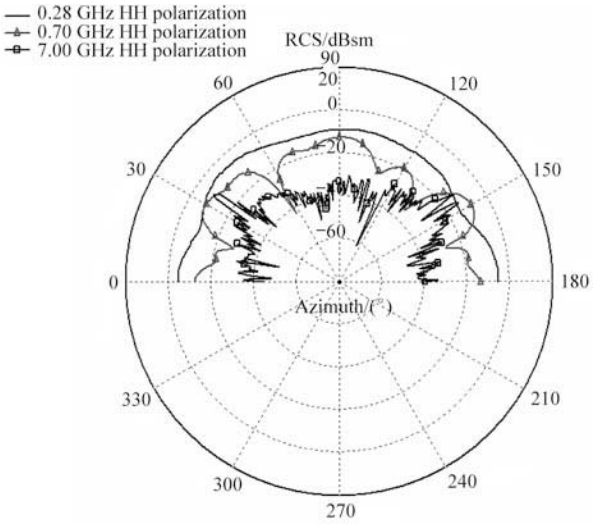

Fig.4 Multi-frequency RCS curves of Configuration 3.

Fig.4 shows that the RCS curve is complex and oscillates significantly in the high-frequency zone because the whole aircraft shape has an important influence on RCS. In the resonance zone, the RCS curve oscillates in an unsteady rhythm, and the aircraft shape will affect its RCS distribution due to the superposition of all parts at different phases. In the Rayleigh zone, the RCS curve oscillates slightly and the effect of shape on RCS is weakened.

Therefore, the aircraft shape has different effects on RCS distribution in three frequency zones, and it is necessary to investigate the multi-frequency reduction characteristics of shape stealth so that the effective techniques can be provided for aircraft stealth design.

4.2. Analysis of multi-frequency RCS reduction characteristics of shape stealth

Shape stealth tries to optimize the aircraft layout to achieve the goal of RCS reduction. Take Configuration 1 as a reference, the reduction characteristics of Configurations 2-3 are investigated. As for the similarity of

scattering under VV and HH polarizations, the characteristics of HH polarization are chosen for detailed analysis. Suppose $\eta = d/\lambda$ is the typical electrical size, where d is the aircraft's typical geometrical size.

Fig.5 shows the RCS AM curves of the three configurations changing with frequencies for 0°-30° and 0°-180° angle zones. In Fig.5, we can see that the RCS AM values of all the configurations assume being oscillated when the frequency is increased. For the 0°-30° angle zone, the RCS AM value is increased rapidly in the Rayleigh zone and decreased in the high-frequency zone. The RCS AM value of Configuration 1 is the highest one and that of Configuration 3 is the lowest one. This means that Configuration 3 can provide the best stealth performance.

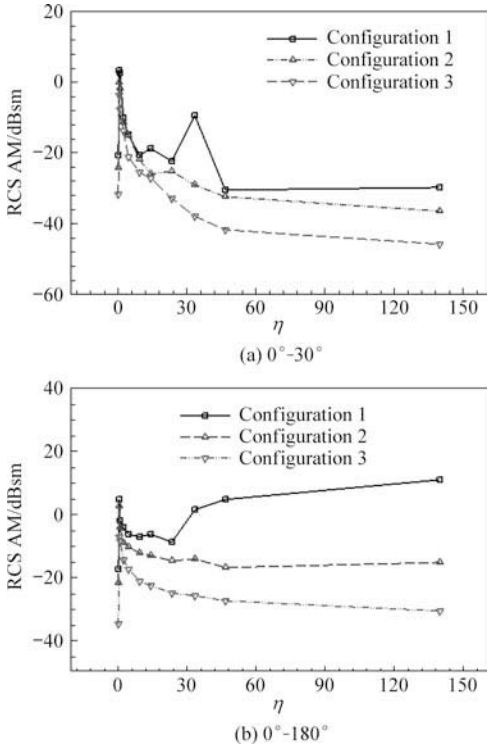

Fig.5 RCS AM curves with different η.

It can be seen from Fig.5, Configurations 2-3 exhibit a reduction effect under HH polarization as compared to Configuration 1. The reduction effects of these two configurations are remarkable in the high-frequency and resonance zones. Furthermore, the stealth performance is disappeared for Configuration 2 and is weakened for Configuration 3 in the Rayleigh zone.

Although both of these configurations show RCS reduction effects in the high-frequency and resonance zones, Configuration 3 achieves higher excellence in stealth performance in multi-frequency zones than Configuration 2 does due to the flying wing layout. It becomes clear that the concept of shape stealth can be used to design aircraft with high stealth performance owing to the multi-frequency RCS reduction of shape stealth.

For different frequencies, the RCS reduction effect of shape is different: the shape stealth performance is enhanced when the incident wave frequency is increased, and the RCS reduction will be most significant in the high-frequency zone.

In general, a narrow-band RCS reduction will be achieved for radar absorbing materials. When the frequency falls outside of the band (i.e. being greater or smaller than the design frequency), the reduction effect will be significantly diminished and the RCS can be increased. In addition, the radar absorbing materials may increase aircraft weight, decrease payload, and reduce the operational effectiveness.

However, a better multi-frequency RCS reduction effect can be obtained through shape stealth to meet the future stealth requirements in multi-frequency or all frequencies. Only in the Rayleigh zone the RCS reduction effect will be decreased. These multi-frequency RCS reduction characteristics can play an important role in aircraft stealth design, sufficiently compensate for the deficiencies of radar absorbing materials and improve the overall performance of stealth aircraft.

5. Conclusions

Three new control factors are proposed, which will be varied according to the process and the number of integral samples. Their effects on the number of integral samples and the precision of MLFMA are discussed. A new approach employing control factors is presented to improve the efficiency and save the memory while having the same precision achieved by the traditional approaches. Both the validity and accuracy of the improved MLFMA are confirmed through computational examples.

Using improved MLFMA, the multi-frequency RCS reduction characteristics of the whole aircraft are investigated, and the shape effects on RCS in different frequency zones are presented. It is shown that the shape stealth possesses multi-frequency RCS reduction effect that is significant in the high-frequency and resonance zones, but is weaker in the Rayleigh zone. Compared with material stealth, shape stealth offers greater advantages of improving the stealth performance of aircraft.

References

[1] Liu Z H, Huang P L, Wu Z, et al. Analysis of scattering from serrated edge plate on aircraft with MLFMA. Journal of Beijing University of Aeronautics and Astronautics 2008; 34(5): 499-502. [in Chinese]

[2] He K F, Qian W Q, Chen J Q, et al. Integrated aircraft design of aerodynamic and stealthy performance with numerically solving fluid dynamics and electromagnetics equations. Acta Aerodynamic Sinica 2009; 27(2): 180-185. [in Chinese]

[3] Sun Y F, Xu S J. The application of asymptotic waveform evaluation technique in fast analysis of the three

dimensional electromagnetic scattering. Acta Electronica Sinica 2002; 30(6): 794-796. [in Chinese]
[4] Gao Z H, Wang M L. An efficient algorithm for calculating aircraft on the geometrical characteristics. Chinese Journal of Aeronautics 2008; 21(4): 296-303.
[5] Zhang Z B, Chen Y L, Gao Z H. MLFMA for solution of 3D complex object. Journal of Nanjing University of Aeronautics & Astronautics 2007; 39(2): 222-226. [in Chinese]
[6] Hu J, Nie Z P, Que X F, et al. Fast computation of scattering from 3D complex structures by MLFMA. Journal of Systems Engineering and Electronics 2008; 19(5): 872-877.
[7] Song J M, Lu C C, Chew W C. Multilevel fast multipole algorithm for electromagnetic scattering by large complex objects. IEEE Transactions on Antennas and Propagation 1997; 45(10): 1488-1493.
[8] Liu Z H, Wu Z, Zhou J, et al. Improving multilevel fast multipole algorithm. Acta Aeronautica et Astronautica Sinica 2008; 29(5): 1180-1185. [in Chinese]
[9] Song J M, Chew W C. Fast multipole method solution of three dimensional integral equation. IEEE Transactions on Antennas and Propagation 1995; 43(10): 1528-1531.
[10] Liu Z H, Huang P L, Wu Z. Frequency response scattering characteristic of aircraft. Acta Aeronautica et Astronautica Sinica 2009; 30(4): 643-648. [in Chinese]
[11] Wang H G. Research on rigorous modeling and high efficient algorithms for 3D EM scattering by large object with open cavities. PhD thesis, University of Electronic Science & Technology of China, 2001. [in Chinese]
[12] Rao S M, Wilton D R, Glisson A W. Electromagnetic scattering by surfaces of arbitrary shape. IEEE Transactions on Antennas and Propagation 1982; 30(3): 409-419.
[13] Özgur E, Levent G. Enhancing the accuracy of the interpolations and anterpolations in MLFMA. IEEE Transactions on Antennas and Propagation 2006; 54(12): 3822-3826.
[14] Song J M, Chew W C. Interpolation of translation matrix in MLFMA. Microwave and Optical Technology Letters 2001; 30(2): 109-114.
[15] Wen J, Hu J, Nie Z P. A novel strategy of the multipole numbers of the MLFMA. Digital Object Identifier APMC. Piscataway: IEEE, 2005; 4-7.
[16] Song J M, Chew W C. Error analysis for the truncation of multipole expansion of vector Green's function. IEEE Microwave and Wireless Components Letters 2001; 11(2): 311-313.

Biography:

Liu Zhanhe Born in 1977, he received M.S. degree from Northwestern Polytechnical University in 2004 and Ph.D. degree from Beijing University of Aeronautics and Astronautics in 2008. He focuses his academic interests on stealth aircraft design and RCS computation.
E-mail: nwpulzh@163.com